

## Structure-Based Design of a Potent, Selective, and Brain Penetrating PDE2 Inhibitor with Demonstrated Target Engagement

Peter Buijnsters,<sup>\*,†</sup> Meri De Angelis,<sup>‡</sup> Xavier Langlois,<sup>†</sup> Frederik J. R. Rombouts,<sup>†</sup> Wendy Sanderson,<sup>§</sup> Gary Tresadern,<sup>§</sup> Alison Ritchie,<sup>||</sup> Andrés A. Trabanco,<sup>‡</sup> Greet VanHoof,<sup>§</sup> Yves Van Roosbroeck,<sup>†</sup> and José-Ignacio Andrés<sup>‡</sup>

<sup>†</sup>Neuroscience Medicinal Chemistry, Janssen Research & Development, a Division of Janssen Pharmaceutica NV, Turnhoutseweg 30, 2340 Beerse, Belgium

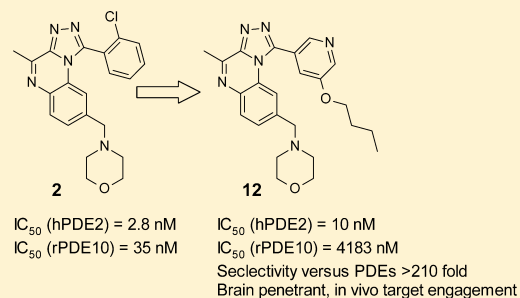
<sup>‡</sup>Neuroscience Medicinal Chemistry, Janssen Research & Development, Janssen-Cilag S.A., C/Jarama 75, 45007 Toledo, Spain

<sup>§</sup>Discovery Sciences, Janssen Research & Development, a Division of Janssen Pharmaceutica NV, Turnhoutseweg 30, 2340 Beerse, Belgium

<sup>||</sup>BioFocus, Chesterford Research Park, Saffron Walden, Essex CB10 1XL, U.K.

## Supporting Information

**ABSTRACT:** Structure-guided design led to the identification of the novel, potent, and selective phosphodiesterase 2 (PDE2) inhibitor **12**. Compound **12** demonstrated a >210-fold selectivity versus PDE10 and PDE11 and was inactive against all other PDE family members up to 10  $\mu$ M. *In vivo* evaluation of **12** provided evidence that it is able to engage the target and to increase cGMP levels in relevant brain regions. Hence, **12** is a valuable tool compound for the better understanding of the role of PDE2 in cognitive impairment and other central nervous system related disorders.



**KEYWORDS:** PDE2 inhibitor, target engagement, phosphodiesterase 2, [1,2,4]triazolo[4,3-a]quinoxalines

Phosphodiesterases (PDEs) play a critical role in the degradation of the cellular levels of the secondary messengers cAMP (3',5'-cyclic adenosine monophosphate) and cGMP (3',5'-cyclic guanosine monophosphate).<sup>1</sup> To date 11 different PDEs are known and are characterized by the cyclic nucleotide substrate that they hydrolyze: PDE4, 7, and 8 hydrolyze cAMP, and PDE5, 6, and 9 hydrolyze cGMP, whereas PDE1, 2, 10, and 11 hydrolyze both substrates. Both cAMP and cGMP play a key role in intracellular signaling and in processes of neuroplasticity such as long-term potentiation (LTP),<sup>2,3</sup> which could result in improved cognitive function and memory.<sup>4</sup> Thus, PDE inhibition is of interest in the treatment of cognitive dysfunction.<sup>5</sup>

PDE2 expression is highest in the brain, where it is mainly localized in the cortex, hippocampus, and striatum.<sup>6</sup> This suggests that PDE2 may regulate intraneuronal cGMP and cAMP levels in brain areas involved in emotion, perception, concentration, learning, and memory. The main evidence was generated with 2-[(3,4-dimethoxyphenyl)methyl]-7-[1-[(1R)-1-hydroxy ethyl]-4-phenyl-butyl]-5-methyl-3H-imidazo[5,1-f]-[1,2,4] triazin-4-one, Bay 60-7550 (**1**),<sup>7</sup> a highly selective PDE2 inhibitor, but with suboptimal pharmacokinetic (PK) properties. Several studies have postulated that **1** improved memory acquisition and consolidation in object recognition tasks in rats.<sup>8–11</sup> However, a recent study demonstrated poor brain uptake of **1** in rats 30 min after administration of a 10 mg/

kg oral dose ( $B/P = 0.05$ ,  $[P] = 72.9$  ng/mL, and  $[B] = 3.6$  ng/g), meaning that *in vivo* data with this compound should be treated with caution.<sup>11</sup> We recently reported the identification and early optimization of [1,2,4]triazolo[4,3-a]quinoxalines as dual PDE2/PDE10 inhibitors, culminating in the identification of compound **2**, a potent PDE2/PDE10 inhibitor ( $IC_{50}$  2.8 nM for PDE2 and 35 nM for PDE10) (Figure 1).<sup>12</sup>

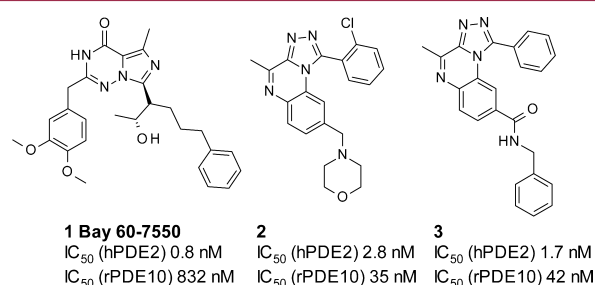


**Figure 1.** Structure and PDE2/PDE10 inhibitory activity of Bay 60-7550 **1** and [1,2,4]triazolo[4,3-a]quinoxalines **2** and **3**. All data was generated at Janssen.

Received: June 23, 2014

Accepted: July 22, 2014

Published: July 22, 2014

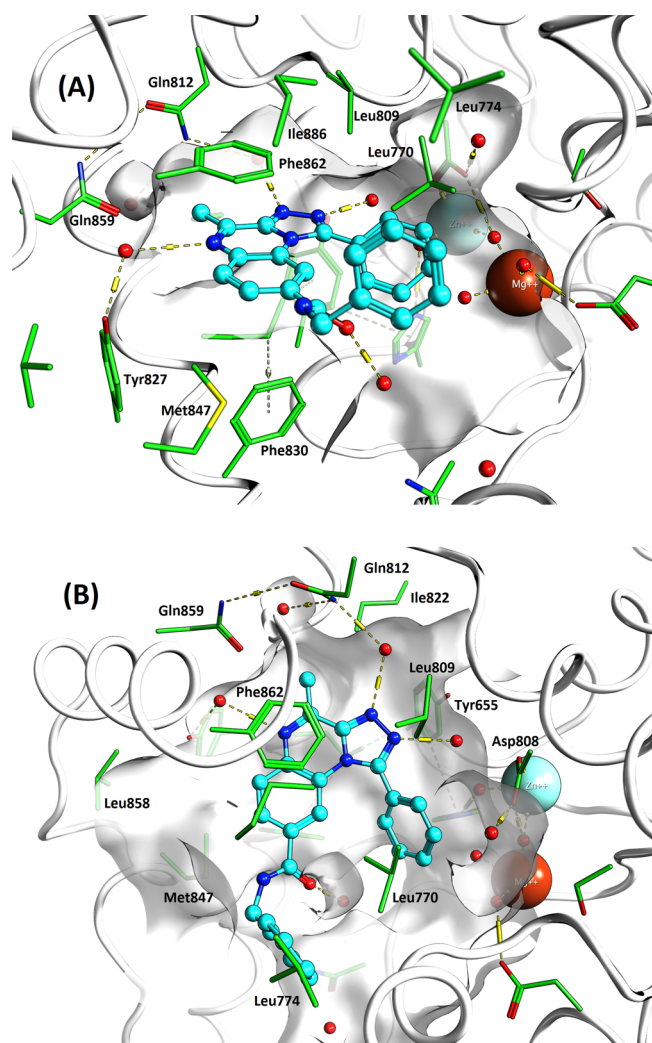


**Figure 2.** X-ray crystallographic binding mode of **3** (cyan) with PDE2A viewed from the entrance to the active site (A) and top down (B); pdb accession code 4D09. Important amino acids are highlighted in green, and catalytic  $Zn^{2+}$  and  $Mg^{2+}$  ions are shown, along with active site water molecules (red spheres).

In this letter we report the crystal structure of **3**, as well as the structure-guided optimization of **2** and **3** toward a suitable tool compound for further validation of PDE2 as a target for treatment of cognitive disorders. The goal was to identify a probe molecule that should (1) be 100-fold selective for PDE2 versus all other PDE family members; (2) have reasonable brain exposure; and (3) have good physicochemical properties.

At the outset of our work only two PDE2 crystal structures were available in the public domain.<sup>13,14</sup> These structures showed PDE2 folds similar to other PDEs with shared binding site features: a conserved glutamine enables binding to the nucleobase, the sulfate extends across the site and interacts with the catalytic metals. It was recognized that structure-based optimization would benefit greatly from a crystallographic structure of our tricyclic hit series. The structure of **3** bound to the PDE2A catalytic domain (amino acids 579–921) was successfully determined and refined to 2.5 Å resolution ( $R_{work} = 21.8\%$  and  $R_{free} = 29.8\%$ ). Binding of **3** sits in the traditional hydrophobic clamp between Phe830 and Phe862. The binding mode is unique as the ligand interacts with multiple water molecules within the active site. Interestingly, the ligand forces

the conserved glutamine (Gln859) into an alternative conformation compared to most PDE structures.

Consequently, space exists for a water molecule to form a hydrogen bond bridge between the quinoxaline and the conserved glutamine. In addition, a methyl is in the typical position occupied by hydrogen bonding groups of substrate cAMP or cGMP. The triazolo group of the ligand forms hydrogen bonds to two different PDE-conserved water molecules, which in turn H-bond to enzyme amino acids including Tyr655 and Gln812. The *N*-benzylamide is located at the site entrance and hugs the roof of the pocket interacting with lipophilic amino acids Leu770 and Leu774. The planarity of the amide with the tricyclic scaffold is broken (carbonyl oxygen is  $36^\circ$  out of plane) to avoid a clash between the amide NH and benzylic carbon atom with Met847. Another ligand solvent H-bond interaction between the carbonyl oxygen to a highly conserved water molecule likely compensates for the internal ligand strain. This suboptimal conformation was therefore a candidate for optimization. The phenyl substituent on the triazole also interacts with Leu770. It was noticed that the water molecule interacting with the amide carbonyl could be targeted from this aromatic ring. Changing the phenyl to a 3-pyridyl would permit the  $sp^2$  nitrogen to form a hydrogen bond to this water molecule. In summary, structural analysis of **3** provided rationale for structural modifications at both substituent positions on the tricycle.

Docking of **1** into the apo-PDE2 structure (1Z1L) available at the time provided a structural understanding of the high selectivity (PDE10/PDE2 = 1000). Subsequently the experimental structure of Zhu et al.<sup>15</sup> confirmed that the 3-phenylpropyl substituent of the asymmetric center accesses an open pocket above the active site. This uncommon interaction for PDEs is the source of the high selectivity for **1**. In other PDE structures, such as PDE10 2O8H,<sup>16</sup> this channel is blocked by the closer proximity of Leu625 and Leu665 (Leu770 and Leu809 in PDE2).

To achieve PDE2 selectivity, a small number of molecules were designed. First, replacement of the benzylamide in **3** with *N*-morpholinylmethyl was previously shown to be an optimal group at this position.<sup>12</sup> Second, an *ortho*-halogen on the aryl substituent of the triazole favors an orthogonal orientation with respect to the tricycle and reduces rotational freedom providing energetic gains for binding (Figure 3). From this twisted phenyl/

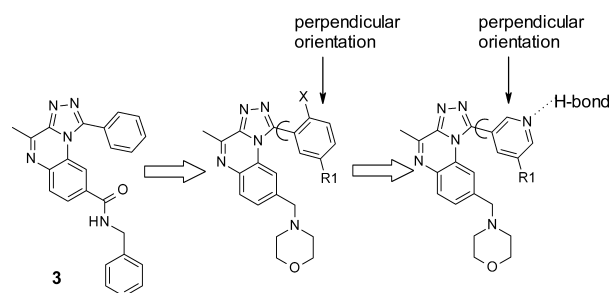


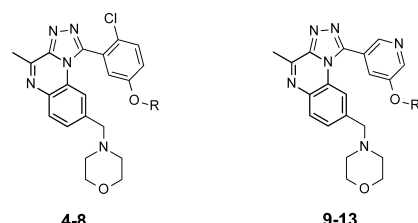
**Figure 3.** Design principles for novel compounds from compound **3**.

aryl group the selectivity pocket is accessible by a suitable substituent on the same ring. Third, replacing phenyl with a 3-pyridyl directs the aromatic nitrogen to interact with the conserved water molecule, helping the aromatic ring adopt the preferred twisted orientation without an *ortho* substituent. In

turn, a lipophilic moiety in the 5 position of the pyridyl accesses the lipophilic pocket and enhances selectivity versus PDE10.

*In vitro* hPDE2 and rPDE10 inhibition for target compounds<sup>12,17</sup> along with the PDE10/PDE2 selectivity ratio are shown in Table 1. In general the *o*-chlorophenyl substituted

**Table 1.** *In Vitro* hPDE2 and rPDE10 Inhibitory Activity of Compounds 2 and 4–13 and Their PDE10/PDE2 ratio



compd	R	IC <sub>50</sub> (nM) <sup>b</sup>		
		hPDE2	rPDE10	PDE10/PDE2
2	N/A <sup>a</sup>	2.8	35	13
4	Me	10.4	106	10
5	Et	6.1	266	44
6	<i>n</i> -Pr	6.5	322	50
7	<i>i</i> -Pr	4.8	1862	388
8	<i>n</i> -Bu	7.7	1622	211
9	Me	12.1	271	22
10	<i>n</i> -Pr	30.5	6131	201
11	<i>i</i> -Pr	404	>10000	>25
12	<i>n</i> -Bu	10.1	4823	482
13	MeOCH <sub>2</sub> CH <sub>2</sub>	123	7762	63

<sup>a</sup>Not available. <sup>b</sup>IC<sub>50</sub>s were calculated from at least three independent experiments. See Supporting Information for details.

compounds 4–8 had similar PDE2 potency as examples 2 and 3, and their selectivity versus PDE10 improved as the lipophilic character of the aliphatic chain increases (8 *n*-Bu > 6 *n*-Pr > 5 Et > 4 Me). With regard to PDE10/PDE2 selectivity, the linear *n*-butyl chain (8) seemed slightly worse compared with the branched isopropyl moiety (7). The PDE2 affinity for pyridyl derivatives such as 9, 10, and 12 was similar to their corresponding *o*-chloro analogues 4, 6, and 8, and selectivity improved again with increasing chain length in the alkoxy substituent. Thus, compound 12 containing an *n*-butyloxy substituent possesses remarkable 480-fold selectivity for PDE2 versus PDE10. Introduction of polar groups in the aliphatic chain or branching was detrimental for potency and selectivity as can be seen for compounds 13 and 11.

Generally, there was a trend for the pyridyl derivatives being less potent than the *o*-chloro substituted molecules. This may arise from the rotational freedom of the pyridyl derivatives versus the *o*-chlorophenyl substituted tricycles. One exception was compound 12, which maintained good PDE2 activity of 10.1 nM and 480-fold selectivity versus PDE10. The structure of compound 12 in complex with PDE2 was determined and refined to 1.9 Å and confirmed our design hypothesis (Figure 4;  $R_{\text{work}} = 20.5\%$  and  $R_{\text{free}} = 24.7\%$ ).

Molecule 12 sits in the usual hydrophobic clamp between Phe830 and Phe862 and the conserved glutamine and adopts a conventional conformation interacting closely to the scaffold forming a hydrogen bond to the quinoxaline nitrogen at a 2.2 Å distance. The hydrogen bonds between the nitrogen atom of the pyridyl moiety and the water in the bottom of the active site helps the pyridyl adopt the rotational conformation permitting the 5-

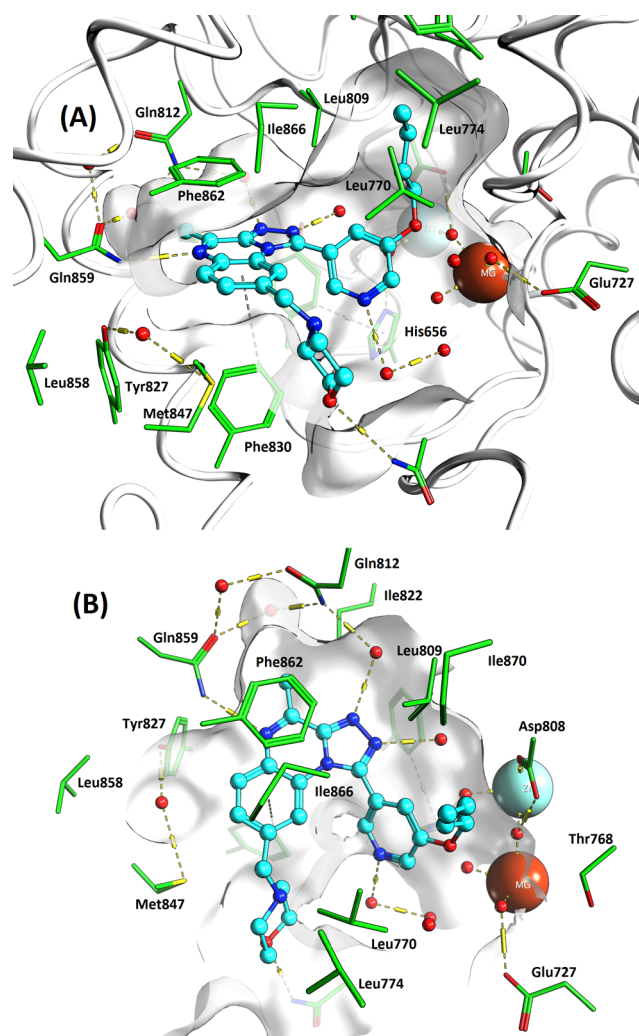


**Figure 4.** X-ray crystallographic binding mode of 12 (cyan) with PDE2A viewed from the entrance to the active site (A) and top down (B); pdb accession code 4D08. Annotation and coloring is the same as Figure 2

butyloxy-group to access the lipophilic pocket. Compared to the structure of 3, 12 displaced a water molecule from this pocket, which is formed by hydrophobic residues such as Leu770, Leu809, and Ile866, explaining the preference for lipophilic alkyl chains. The conformational locking of the pyridyl rotation via the water mediated H-bond may only be successful with optimal 5-position substitution as shown by the greater variability in the PDE2 activity of the pyridyl analogues compared to the *o*-chlorophenyl examples. The morpholine group in 12 goes to the bottom of the active site, and its flexibility is represented in subtly different conformations in the different crystallographic subunits. In one of the four subunits the morpholine oxygen is able to form a hydrogen bond with Asn704. The triazole forms the same hydrogen bond interactions to two water molecules as seen in 3. Conversely, in the X-ray structure of PDE2 with molecule 3 (Figure 2), the selectivity pocket is closed. This highlights the value of using both the X-ray structure of 3 to confirm the [1,2,4]triazolo[4,3-*a*]quinoxaline scaffold binding mode along with the docking of 1 into apo-PDE2 to reveal the selectivity pocket. Along with the recent work of Zhu et al.<sup>15</sup> we provide here additional evidence showing selective PDE inhibitors accessing this unusual ligand-induced hydrophobic pocket.

Compound **12** was tested for inhibition against other PDE enzymes and *in vitro* ADME assays to evaluate its potential as a candidate for *in vivo* studies. Compound **12** demonstrated >210-fold selectivity versus PDE10 and PDE11, and it was inactive against other PDE family members (Table 2).

**Table 2. PDE Profile of Compound 12**

subtype	IC <sub>50</sub> (nM) <sup>a</sup>	subtype	IC <sub>50</sub> (nM) <sup>a</sup>
hPDE1A	>10000	hPDE6AB	>10000
hPDE2A	10	hPDE7A	>10000
hPDE3B	>10000	hPDE9A	>10000
hPDE4D	>10000	rPDE10A	4823
hPDE5A	>10000	hPDE11A	2138

<sup>a</sup>IC<sub>50</sub>s were calculated from experiments each with eight concentrations.

Molecule **12** had high metabolic turnover (Table 3, first two entries), which prevents oral administration. The compound was

**Table 3. In Vitro ADME and Physicochemical Properties of Compound 12**

<i>in vitro</i> ADME and physicochemical properties	
hLM	0 <sup>a</sup>
rLM	0 <sup>a</sup>
formulatability (mg/mL)	4, <sup>b</sup> 15, <sup>c</sup> 16 <sup>d</sup>
CYP450 <sup>e</sup>	>10 μM
AMESII <sup>f</sup>	inactive, <125 μg/mL <sup>f</sup>

<sup>a</sup>Percent of compound remaining after 15 min incubation with rat or human liver microsomes. <sup>b</sup>Water pH 3.6. <sup>c</sup>Ten percent β-HP-CD at pH 3.6. <sup>d</sup>Twenty percent HP-β-CD at pH 7.0. <sup>e</sup>Inhibition of cytochrome P450 (CYP) enzyme activity in the presence of test compound at 1 μM; 1A2, 2C9, and 2D6, CYP inhibition measured using the recombinant CYP inhibition screening assay, 10 μM test compound; 2C19 and 3A4, CYP inhibition measured using the human liver microsomal CYP inhibition assay, IC<sub>50</sub> determination. <sup>f</sup>AMESII: *in vitro* colorimetric mutagenicity assay using an adaptation of the AMESII Mutagenicity Assay kit from Xenometric.

inactive in a bacterial mutagenicity assay (AMESII). The poor *in vitro* microsomal stability of **12** translated to rapid clearance from rat plasma after i.v. injection (*t*<sub>1/2</sub> = 0.31 h, Cl >100% of rat hepatic blood flow, Table 5).

Nevertheless, a concentration of 658 ± 34 ng/mL in plasma was reached after s.c. administration of a 10 mg/kg dose of **12** (Table 5). Compound **12** displayed brain penetration with a B/P ratio of approximately 1 over several hours (Table 4). Furthermore, even after 4 h, promising brain levels could be measured. In order to have an estimation of the free

**Table 4. Pharmacokinetic Parameters for Compound 12<sup>a</sup>**

time (h)	plasma (ng/mL) ± SD	brain (ng/g) ± SD	B/P
0.5	663 ± 34	932 ± 105	1.4
1	730 ± 49	824 ± 40	1.1
2	680 ± 50	777 ± 124	1.1
4	259 ± 138	269 ± 117	1.1
7	78 ± 63	119 ± 40	0.93
24	B.Q.L. <sup>b</sup>	B.Q.L. <sup>b</sup>	n.d. <sup>c</sup>

<sup>a</sup>Male Sprague–Dawley rat fed (*n* = 3) 10 mg/kg s.c., 1 mg/mL in 20% HP-β-CD, pH = 7.0. <sup>b</sup>B.Q.L. = below quantification level. <sup>c</sup>n.d. = not determined.

**Table 5. Brain Exposure Profile of 12 after s.c. Administration<sup>a</sup>**

<i>in vivo</i> plasma kinetics in rat <sup>a</sup> 2.5 mg/kg i.v. mean (±SD)	
<i>t</i> <sub>1/2</sub> (h)	0.31(±0.02)
Cl (L/h/kg)	7.8 (±1.3)
<i>V</i> <sub>dss</sub> (L/kg)	2.7 (±0.2)
AUC <sub>0-inf</sub> (ng·h/mL)	305 (±54)
<i>in vivo</i> plasma kinetics in rat <sup>a</sup> 10 mg/kg s.c. mean (±SD)	
<i>t</i> <sub>1/2</sub> (h)	1 (±0.1)
<i>C</i> <sub>max</sub> (ng/mL)	658 (±34)
<i>t</i> <sub>max</sub> (h)	0.67 (±0.29)
AUC <sub>0-inf</sub> (ng·h/mL)	1671 (±90)

<sup>a</sup>Male Sprague–Dawley rat fed (*n* = 3), 10 mg/kg, 1 mg/mL in 20% HP-β-CD, pH = 7.0.

concentration in brain, the unbound brain fraction (*F*<sub>ub</sub>) and the unbound fraction to plasma proteins (*F*<sub>up</sub>) were determined, which amounted to 0.14 and 0.31, respectively. This then results in a free concentration of **12** in the brain of 115 ng/g (67 nM) at 1 h postdose.

Next, an *ex vivo* occupancy assay was used to evaluate PDE2 target engagement in rat brain slices using tritiated **12** as an autoradiolabeling agent. Coadministration of **12** and MP10<sup>17</sup> (2.5 mg/kg, s.c.), a potent and selective PDE10 inhibitor, which increases the signal-to-noise ratio, demonstrated that **12** occupies PDE2 with an ED<sub>50</sub> of 4.3 mg/kg (Figure 5), which corresponds

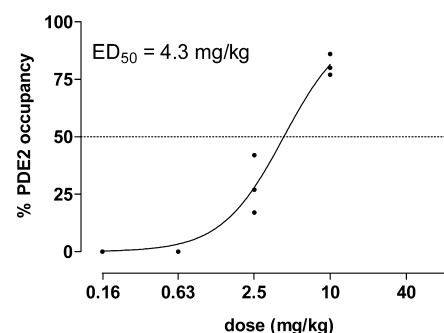


**Figure 5.** *In vivo* PDE2 receptor occupancy against dosage of **12**. Male Wistar rats (*n* = 3 per dose). Occupancy was calculated as the inhibition of specific [<sup>3</sup>H]-**12** binding in drug-treated animals relative to vehicle-treated animals.

to an EC<sub>50</sub> of 21 nM. The increase of the signal-to-noise ratio can be explained by the fact that PDE10 inhibition increases intracellular cGMP, which is known to activate PDE2 through its GAF domain. To confirm target engagement and central functional effect, the levels of cyclic nucleotides versus baseline concentrations were determined in rat striatum and hippocampus, regions involved in learning and memory. One hour after dosing of **12** at 10 mg/kg s.c., cGMP levels increased in rat striatum with 251% (range 186%–302%) compared to vehicle-dosed animals over 5 independent experiments (*n* = 4–5 each). The cAMP levels did not consistently increase (mean change 109%, range 82%–139%). The same profile was observed in hippocampus with a significant increase in cGMP levels (298%) and unchanged cAMP (91%) levels (one experiment, *n* = 5). These data are in agreement with prior evidence that PDE2 inhibition in brain mainly influences cGMP levels rather than cAMP.<sup>10,18</sup>

In summary, structure-based design optimized a series of [1,2,4]triazolo[4,3-*a*]quinoxalines for their activity against PDE2 and selectivity versus PDE10. Crystallographic structures along with docking of known selective molecules provided rationale for synthesis. The most selective example, **12**, displayed 10.1 nM inhibition against PDE2, >210-fold selectivity versus PDE10 and PDE11, and was inactive against other PDEs. X-ray crystallography confirmed our design hypotheses that **12** accesses an unusual ligand-induced lipophilic pocket. Molecule **12** displayed an acceptable *in vitro* ADME and physicochemical profile and good brain exposure. More importantly, **12** showed target engagement by occupying PDE2 and increasing cyclic nucleotide levels in relevant rat brain regions. Molecule **12** thus represents a valuable probe compound for further studies of the role of PDE2 in central nervous system related disorders.

## ■ ASSOCIATED CONTENT

### 📄 Supporting Information

Docking protocols for Bay 60-7550 (**1**), protocols of *in vitro* hPDE2 inhibitory activity of final compounds **4–13**, *in vitro* PDE profile of **12**, *in vivo* PDE2 occupancy method, *in vivo* cAMP and cGMP measurements in striatum and hippocampus, brain tissue binding, plasma tissue binding, synthesis procedures, and characterization. This material is available free of charge via the Internet at <http://pubs.acs.org>.

## ■ AUTHOR INFORMATION

### Corresponding Author

\*(P.B.) E-mail: [pbuijnst@its.jnj.com](mailto:pbuijnst@its.jnj.com). Tel: +32(0)14607439.

### Author Contributions

The manuscript was written through contributions of all authors. All authors have given approval to the final version of the manuscript.

### Notes

The authors declare no competing financial interest.

## ■ ACKNOWLEDGMENTS

Lieve Heylen kindly provided support with the retrieval of all *in vitro* and *in vivo* data. We also thank Ilse Lenaerts for performing the occupancy experiments. We thank the ADME-Toxicology department for performing all the ADME experiments.

## ■ ABBREVIATIONS

AUC<sub>0-inf</sub>, area under the curve until infinite time; Cl, clearance; CYP450, cytochrome P450; ED<sub>50</sub>, dose giving 50% effect; HP- $\beta$ -CD, (2-hydroxypropyl)- $\beta$ -cyclodextrin; hLM, human liver microsomes; IC<sub>50</sub>, concentration giving 50% inhibition; *i.v.*, intravenous; pdb, Protein Databank; PK, pharmacokinetic; *p.o.*, *per os*; *s.c.*, subcutaneous; SD, standard deviation; rLM, rat liver microsomes; *t*<sub>1/2</sub>, half-life; *t*<sub>max</sub>, time at maximum concentration; *V*<sub>dss</sub>, steady-state volume of distribution

## ■ REFERENCES

- (1) Maurice, D. H.; Ke, H.; Ahmad, F.; Wang, Y.; Chung, J.; Manganiello, V. C. Advances in targeting cyclic nucleotide phosphodiesterases. *Nat. Rev. Drug Discovery* **2014**, *13*, 290–314.
- (2) Frey, U.; Huang, Y. Y.; Kandel, E. R. Effects of cAMP simulate a late stage of LTP in hippocampal CA1 neurons. *Science* **1993**, *260*, 1661–1664.
- (3) Son, H.; Lu, Y. F.; Zhuo, M.; Arancio, O.; Kandel, E. R. The specific role of cGMP in hippocampal LTP. *Learn. Mem.* **1998**, *5*, 231–245.
- (4) Bernabeau, R.; Schmitz, P.; Faillace, M. P.; Izquierdo, L.; Medina, J. H. Hippocampal cGMP and cAMP are differentially involved in

memory processing of inhibitory avoidance learning. *NeuroReport* **1996**, *7*, 585–588.

(5) Blokland, A.; Menniti, F. S.; Prickaerts, J. PDE Inhibition and cognition enhancement. *Expert Opin. Ther. Pat.* **2012**, *22*, 349–354.

(6) Lakics, V.; Karran, E. H.; Boess, F. R. Quantitative comparison of phosphodiesterase mRNA distribution in human brain and peripheral tissues. *Neuropharmacology* **2010**, *59*, 367–374.

(7) Rutten, K.; Prickaerts, J.; Hendrix, M.; van der Staay, F.-J.; Sik, A.; Blokland, A. Time-dependent involvement of cAMP and cGMP in consolidation of object memory: Studies using selective phosphodiesterase type 2, 4 and 5 inhibitors. *Eur. J. Pharmacol.* **2007**, *558*, 107–112.

(8) Prickaerts, J.; de Vente, J.; Honig, W.; Steinbusch, H. W.; Blokland, A. cGMP, but not cAMP, in rat hippocampus is involved in early stages of object memory consolidation. *Eur. J. Pharmacol.* **2002**, *436*, 83–87.

(9) Boess, F. G.; Hendrix, M.; van der Staay, F.-J.; Erb, C.; Schreiber, R.; van Staveren, W.; de Vente, J.; Prickaerts, J.; Blokland, A.; Koenig, G. Inhibition of phosphodiesterase 2 increases neuronal cGMP, synaptic plasticity and memory performance. *Neuropharmacology* **2004**, *47*, 1081–1092.

(10) Rodefer, J. S.; Saland, S. K.; Eckrich, S. J. Selective phosphodiesterase inhibitors improve performance on the ED/ID cognitive task in rats. *Neuropharmacology* **2012**, *62*, 1182–1190.

(11) Reneerkens, O. A.; Rutten, K.; Bollen, E.; Hage, T.; Blokland, A.; Steinbusch, H. W. M.; Prickaerts, J. Inhibition of phosphodiesterase type 2 or type 10 reverses object memory deficits induced by scopolamine or MK-801. *J. Behav. Brain Res.* **2013**, *236*, 16–22.

(12) Andrés, J.-I.; Buijnsters, P.; De Angelis, M.; Langlois, X.; Rombouts, F.; Trabanco, A. A.; Vanhoof, G. Discovery of a new series of [1,2,4]triazolo[4,3-*a*] quinoxalines as dual phosphodiesterase 2/ phosphodiesterase 10 (PDE2/PDE10) inhibitors. *Bioorg. Med. Chem. Lett.* **2013**, *23*, 785–790.

(13) Pandit, J.; Forman, M. D.; Fennell, K. F.; Dillman, K. S.; Menniti, F. S. Mechanism for the allosteric regulation of phosphodiesterase 2A deduced from the X-ray structure of a near full-length construct. *Proc. Natl. Acad. Sci. U.S.A.* **2009**, *106*, 18225–18230.

(14) Iffland, A.; Kohls, D.; Low, S.; Luan, J.; Zhang, Y.; Kothe, M.; Cao, Q.; Kamath, A. V.; Ding, Y. H.; Ellenberger, T. Structural determinants for inhibitor specificity and selectivity in PDE2A using the wheat germ *in vitro* translation system. *Biochemistry* **2005**, *44*, 8312–8325.

(15) Zhu, J.; Yang, Q.; Dai, D.; Huang, Q. X-ray crystal structure of phosphodiesterase 2 in complex with a highly selective, nanomolar inhibitor reveals a binding-induced pocket important for selectivity. *J. Am. Chem. Soc.* **2013**, *135*, 11708–11711.

(16) Chappie, T. A.; Humphrey, J. M.; Allen, M. P.; Estep, K. G.; Fox, C. B.; Lebel, L. A.; Liras, S.; Marr, E. S.; Menniti, F. S.; Pandit, J.; Schmidt, C. J.; Tu, M.; Williams, R. D.; Yang, F. V. Discovery of a series of 6,7-dimethoxy-4-pyrrolidylquinazoline PDE10A inhibitors. *J. Med. Chem.* **2007**, *50*, 182–185.

(17) Andres, J.-I.; Buijnsters, P.; De Angelis, M.; Langlois, X.; Rombouts, F.; Tranbanco, A. A.; Vanhoof, G.; Guillemont, J.; Bormans, G.; Celen, S.; Vliegen, M. Preparation of (un)labeled 1-aryl-4-methyl-[1,2,4]triazolo[4,3-*a*]quinoxaline derivatives as PDE2 and PDE10 inhibitors for therapy and imaging. PCT Int. Appl. WO 2013000924 A1.

(18) Suvarna, N. U.; O'Donnell, J. M. Hydrolysis of *N*-methyl-D-aspartate receptor stimulated cAMP and cGMP by PDE4 and PDE2 phosphodiesterases in primary neuronal cultures of rat cerebral cortex and hippocampus. *J. Pharmacol. Exp. Ther.* **2002**, *302*, 249–256.